

A thermally/chemically robust and easily regenerable anilato-based ultramicroporous 3D MOF for CO₂ uptake and separation

Noemi Monni,^{a,b} Eduardo Andres-Garcia,^b Katia Caamaño,^b Víctor García-López,^b Juan Modesto Clemente-Juan,^b Mónica Giménez-Marqués,^b Mariangela Oggianu,^a Enzo Cadoni,^a Guillermo Mínguez Espallargas,^{*b} Miguel Clemente-León,^{*b} Maria Laura Mercuri^{*a} and Eugenio Coronado^b

^a Dipartimento di Scienze Chimiche e Geologiche, Università degli Studi di Cagliari, I-09042 Monserrato, Italy

^b Instituto de Ciencia Molecular, Universidad de Valencia, Catedrático José Beltrán 2, 46980 Paterna, Spain

Supporting Information

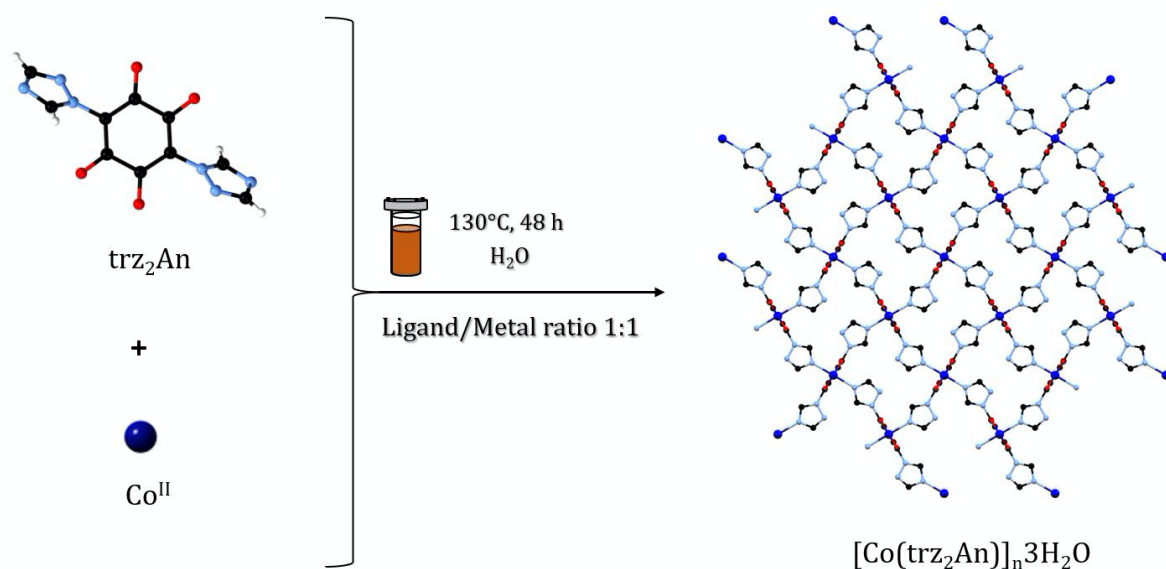
Index

1. Synthesis
2. FT-IR Spectroscopy
3. X-Ray Diffraction
 - a. X-Ray Single Crystal
 - b. Powder X-Ray Diffraction
4. TGA
5. Magnetic Measurements
6. Porosity Measurements and Gas Separation
7. Stability Studies
8. References

1. Synthesis

The 3,6-ditriazoloyl-2,5-dihydroxy-1,4-p-benzoquinone (trz_2An) organic linker was prepared according to the literature.¹ Reagents of analytical grade were purchased from Zentek (TCI) and Sigma Aldrich and used without further purification. Elemental analyses (C, H, and N) were performed with a CE Instruments EA 1110 CHNS.

Synthesis of $[\text{Co}(\text{trz}_2\text{An})]_n \cdot 3\text{H}_2\text{O}$ (1**).** A 5 mL Teflon vial with a mixture of $\text{CoCl}_2 \cdot 6\text{H}_2\text{O}$ (11.9 mg, 0.05 mmol), trz_2An (13.7 mg, 0.05 mmol), NaOH (4 mg, 0.1 mmol) and water (5 mL) was heated at 130°C for 48 hours. After being cooled to room temperature, rectangular dark brown crystals, suitable for an X-Ray Diffraction study, were obtained. Elemental Analysis: *Calcd* % for $\text{C}_{10}\text{H}_{10}\text{N}_6\text{O}_7\text{Co}$ (385.16): C, 31.18; H, 2.62; N, 21.82. *Found*: C, 31.12; H, 2.45; N, 22.00.



Scheme S1. Synthetic strategy for **1**.

2. FT-IR Spectroscopy

FT-IR spectra were performed by using a Bruker Equinox 55 spectrophotometer, preparing the samples as KBr pellets. The spectrum of **1** was collected to be compared with trz_2An . As shown in **Figure S1**, the ν_{CO} stretching vibration typical of free anilate ligand, at 1650 cm^{-1} , and the bands in the region $1550\text{--}1500\text{ cm}^{-1}$ partially disappear and are downshifted due to the coordination of C-O in the MOF.

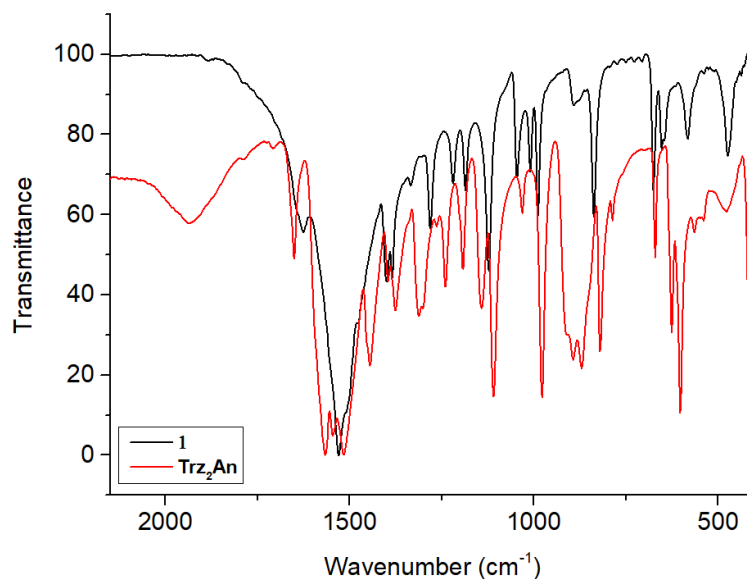


Figure S1. FT-IR spectra of trz_2An (red) and **1** (black) in the $2150\text{-}400\text{ cm}^{-1}$ region.

The characteristic vibrational bands of **1**, along with their assignments, are shown in the following Table.

Table S1. Assignments of characteristic bands for **1**, all the frequencies are in cm^{-1} .²⁻⁵

| Vibrational Modes | Frequency (cm^{-1}) |
|----------------------------|--------------------------------|
| n (C=O) | 1625 |
| n (C=O) + n (C=C) aromatic | 1529 1508 |
| n (aromatic ring) | 1400 1384 |
| n (C-N) | 1280 1122 |
| δ (C=C) | 838 |
| n (Co-O) | 474 |

3. X-Ray Diffraction

a. X-Ray Single Crystal

Single crystals of **1** was mounted on a glass fiber using a viscous hydrocarbon oil to coat the crystal and then transferred directly to the cold nitrogen stream for data collection. X-ray data of **1** were collected at 120 K on a Supernova diffractometer equipped with a graphite-monochromated Enhance (Mo) X-ray Source ($\lambda = 0.710\ 73\ \text{\AA}$). The program CrysAlisPro,

Oxford Diffraction Ltd., was used for unit cell determinations and data reduction. Empirical absorption correction was performed using spherical harmonics, implemented in the SCALE3 ABSPACK scaling algorithm. The structures were solved with the ShelXT structure solution program⁶ and refined with the SHELXL-2013 program,⁷ using Olex2.⁸ Non-hydrogen atoms were refined anisotropically, and hydrogen atoms were placed in calculated positions refined using idealized geometries (riding model) and assigned fixed isotropic displacement parameters. Crystallographic data are summarized in **Table S2**. CCDC-2091526 contains the supplementary crystallographic data for this paper.

Table S2. Crystallographic data for compound **1**

| 1 | |
|---|--|
| Empirical formula | C ₂₀ H ₈ N ₁₂ O ₁₀ Co ₂ |
| Fw | 694.24 |
| Crystal color | brown |
| Crystal size (mm ³) | 0.05 x 0.04 x 0.01 |
| Temperature (K) | 120 |
| Wavelength (Å) | 0.71073 |
| Crystal system, Z | Orthorhombic |
| Space group | Pnmm |
| a (Å) | 9.529(2) |
| b (Å) | 10.157(2) |
| c (Å) | 7.903(2) |
| V (Å ³) | 764.9(3) |
| ρ_{calc} (g.cm ⁻³) | 1.438 |
| $\mu(\text{MoK}\alpha)$ (mm ⁻¹) | 1.144 |
| 2 θ range (°) | 6.532 to 52.934 |
| Index ranges | -11 ≤ h ≤ 11, -12 ≤ k ≤ 12, -9 ≤ l ≤ 9 |
| Reflections collected | 7555 |
| Independent reflections | 800 [R _{int} = 0.1290, R _{sigma} = 0.0857] |
| Data/restraints/parameters | 800/1/59 |
| Goodness-of-fit on F ² | 1.123 |
| Final R indexes [I > 2σ (I)] | R ₁ = 0.1076, wR ₂ = 0.2829 |
| Final R indexes [all data] | R ₁ = 0.1315, wR ₂ = 0.2939 |

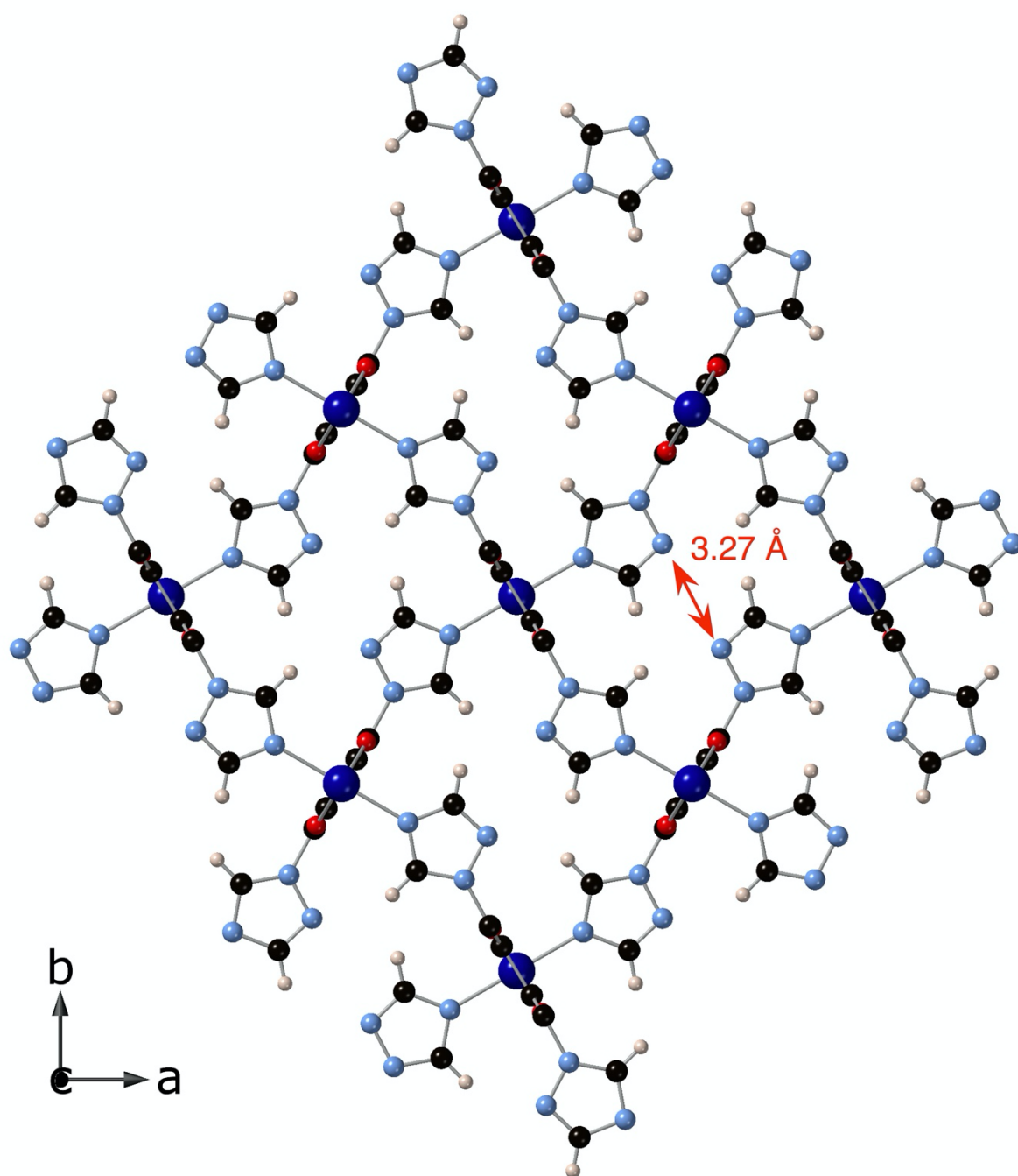


Figure S2. View of the structure of **1** in the *ab* plane with N2-N2 distance. The black, pink, blue, red, and orange spheres represent the C, H, N, O, and Co atoms, respectively.

The distances between triazolyl groups of neighbouring chains, which define the walls of the channels running along the *c* axis, are 3.27 Å (N2-N2 distance) (see **Figure S2**).

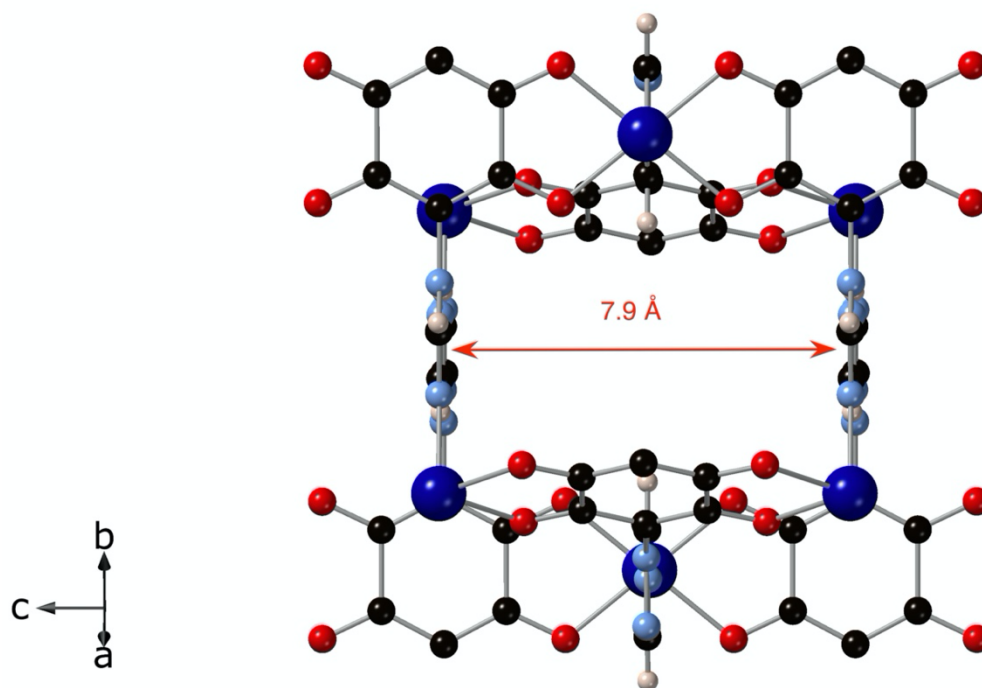


Figure S3. View of the microporous channels orthogonal to the *c*-axis, with distance between the centroids of the parallel triazole rings placed at the walls of these channels. The black, pink, blue, red, and orange spheres represent the C, H, N, O, and Co atoms, respectively.

On the other hand, the distances between the centroids of parallel triazole rings in the channels perpendicular to the *c*-axis are 7.9 Å (see **Figure S3**). The shortest Co intrachain and interchain distances are 7.906 and 8.007 Å, respectively. The distance between two Co^{II} ions from neighbouring chains ions, linked through the triazolyl groups, is 13.297 Å. One molecule of water was found to be disordered over several positions and could not be modelled satisfactorily. It was removed from the electron density map using the OLEX solvent mask command.⁸ Two voids of 90.4 Å³ were found in the unit cell of the filtered crystals occupied by approximately one water molecule (8.7 e⁻), giving a void volume of 23.5%.

Equatorial Co-O and axial Co-N bond lengths are 2.087(5) and 2.094(8) Å, respectively. These distances are similar to those found in 1D chains of formula [Co(CA)(H₂O)₂] \cdot G (CA = chloranilic acid; G = H₂O and phenazine) with Co^{II} in the high spin state.⁹ The C-O distance of 1.257(8) Å in the anilate ligand, the two C-C distances of 1.360(8) and 1.559(15) Å, all together confirm the oxidation state L²⁻ of the anilate ligand.¹⁰

b. Powder X-Ray Diffraction

Powder X-ray diffraction (PXRD) pattern was performed using a 0.7 mm glass capillary filled with polycrystalline samples of the compounds and mounted and aligned on an Empyrean PANalytical powder diffractometer, using Cu K α radiation ($\lambda = 1.54177$ Å). A total of three scans were collected for each compound at room temperature in the 2θ range of 2–40°. Variable temperature PXRD patterns were performed using a θ – θ Bragg–

Brentano focalizing geometry Bruker D8 Avance A25 diffraction system equipped with a Cu K α source ($\lambda = 1.54056 \text{ \AA}$), in the 2θ range of $2\text{--}40^\circ$ and in the temperature range $25\text{--}400^\circ\text{C}$. PXRD pattern of the polycrystalline sample of **1** is perfectly consistent with the calculated pattern (**Figure S4**) confirming the homogeneity and purity of the bulk sample. The thermal stability after activation is confirmed by similar PXRD patterns of the as-synthesized and activated samples (**Figure S5**).

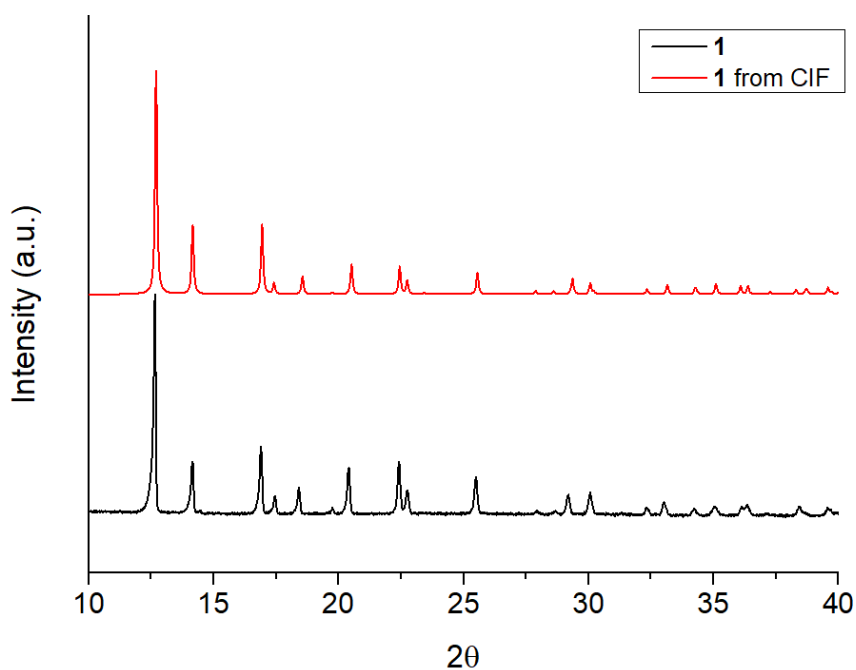


Figure S4. PXRD pattern of compound **1** (black) compared with the calculated from CIF file (red), in the range $10\text{--}40^\circ$.

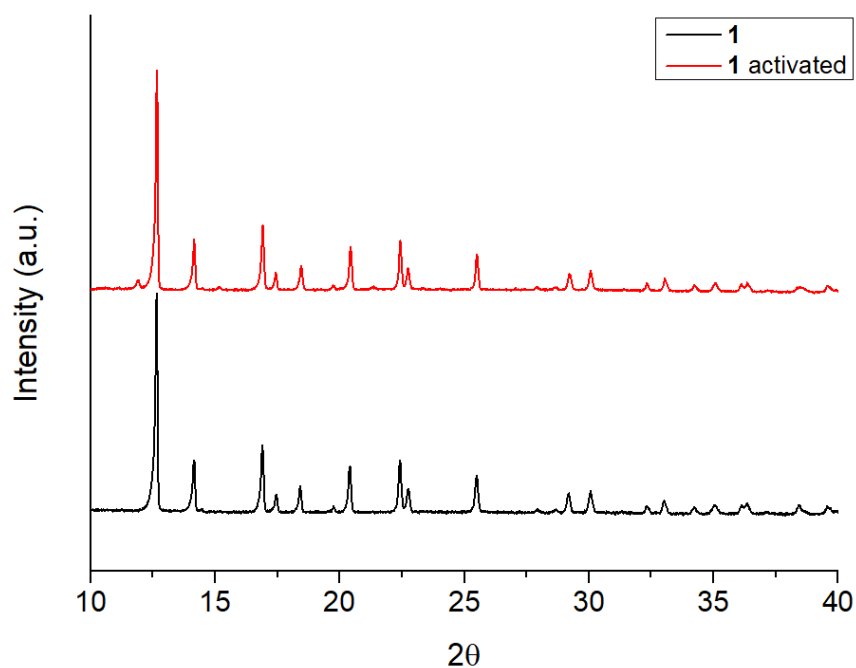


Figure S5. PXRD patterns of compound **1** at RT (red) and **1** after the activation at 150°C (black), in the range $10\text{--}40^\circ$.

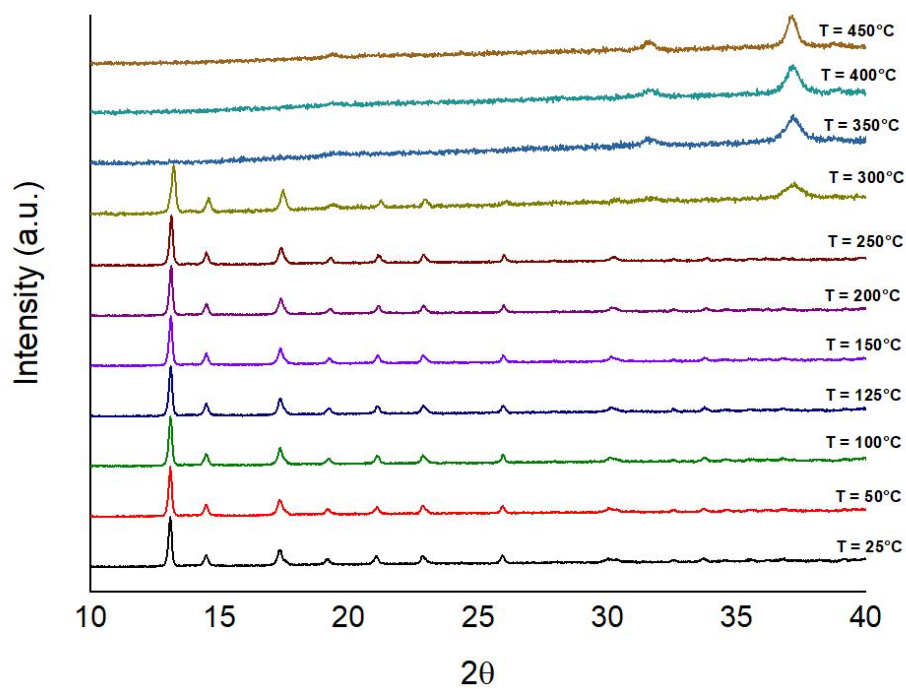


Figure S6. Variable temperature PXRD patterns of compound **1** in the range 10-40°.

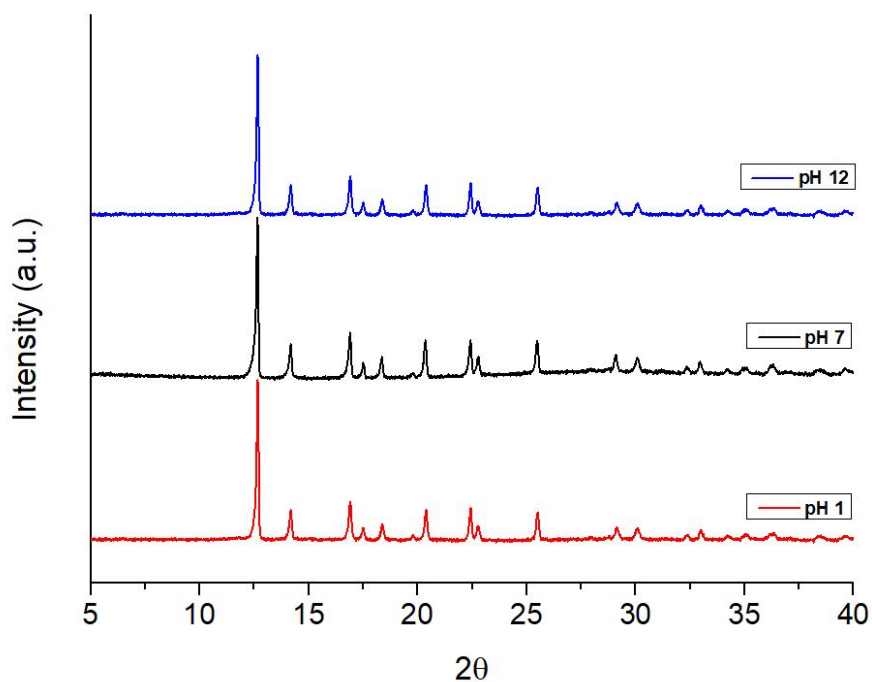


Figure S7. PXRD patterns of **1** after soaking for 24 hours in aqueous solutions of pH = 1, 7 and 12. Concentration: 20 mg of **1** / 20 mL buffer solution.

4. Thermogravimetric Analysis (TGA)

Thermogravimetric analysis was performed in alumina crucibles with the instrument STA-6000 under nitrogen flux (40 mL/min), in the 25-800°C temperature range at 10°C/min.

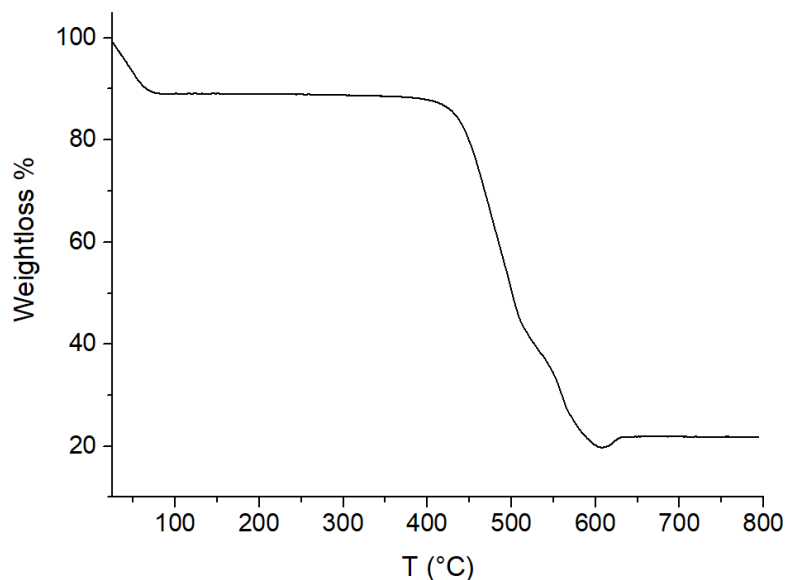
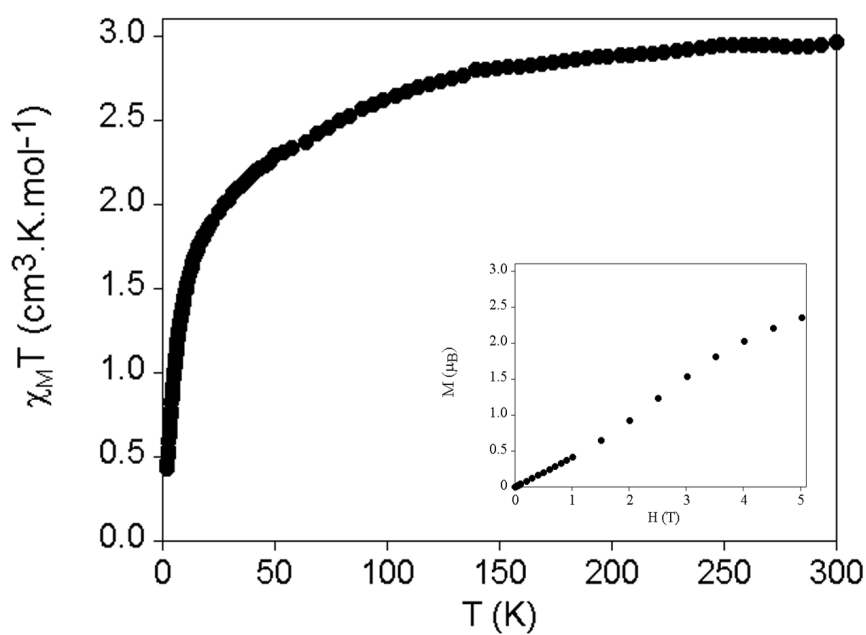


Figure S8. Thermogram of **1** in 25-800°C temperature range.

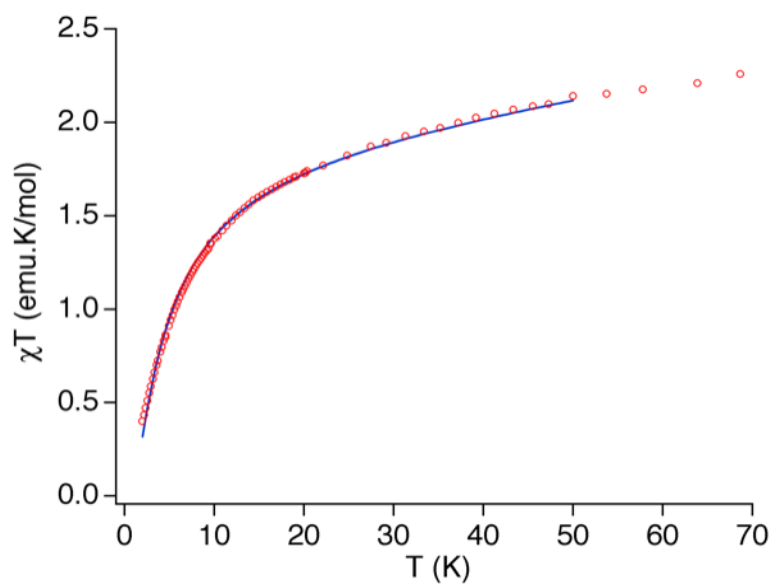
The thermogram of **1** shows a first weight loss of 10.8% at 75°C, which is consistent with the non-coordinated water molecules found in the channels. The system shows very high thermal stability up to 400°C, starting to collapse at $T > 400^\circ\text{C}$ with a ligand degradation.

5. Magnetic Measurements

Magnetic measurements were performed with a Quantum Design MPMS-XL-5 SQUID magnetometer in the 2–400 K temperature range with an applied magnetic field of 0.1 T at a scan rate of 2 K min^{-1} . The thermal dependence of χT product vs temperature of **1**, (**Figure S9**), shows a value of 2.9 $\text{emu}\cdot\text{K}\cdot\text{mol}^{-1}$ at 300 K, which is higher than the spin-only value for a high-spin Co^{II} (d^7) due to considerable orbital momentum contribution to the magnetic moment. Upon cooling, χT decreases continuously with a very abrupt decrease below 100 K to reach a value of 0.4 $\text{emu}\cdot\text{K}\cdot\text{mol}^{-1}$ at 2 K. This is indicative of antiferromagnetic interactions between Co^{II} centers as observed in 1D compounds $[\text{Co}(\text{CA})(\text{H}_2\text{O})_2]\cdot\text{G}$, containing chloranilate ligand.⁹ Indeed, low-temperature data below 50 K can be fitted using the zero-field susceptibility derived by Fisher for the spin-1/2 Ising chain.¹¹ The best set of parameters are: $J = -2.55 \text{ cm}^{-1}$ (for $-2J$ Hamiltonian formalism), $g_z = 7.8$ and $\text{TIP} = 6.5 \times 10^{-3}$. The isothermal field (H) dependence of the magnetization (M) was measured up to 5 T at 2 K (**Figure S9**, Inset). It shows a linear increase at lower magnetic fields as expected for an antiferromagnetic compound. The magnetization at 5 T (2.4 B. M) is significantly lower than the expected saturation for a system with ($S = 3/2$ and $g > 2$).



(a)



(b)

Figure S9. (a) Temperature dependence of $\chi_m T$ of **1**, under an applied field of 0.1 T; Inset: Field dependence of the Magnetization (M-H) measured at 2 K. (b) Low temperature thermal dependence of $\chi_m T$ of **1** (red empty spheres) and best fit of experimental data using the zero-field susceptibility derived by Fisher for the spin-1/2 Ising chain (solid line).

6. Porosity Measurements and Gas Separation

a. Static Isothermal Adsorption Measurements

In order to study the textural properties of the material and its behaviour with the interest gases, low pressure nitrogen and carbon dioxide volumetric isotherms were carried out in a

Tristar II Plus Micromeritics sorptometer, at 77 K and 273 K, respectively. Activation was set at 393 K, under vacuum, for 2 hours.

Although single gas (low-pressure) nitrogen isotherm (77 K) is the most common and standardized adsorption textural characterization measurement, this MOF presents a negligible adsorption curve, as pores from compound **1** are not accessible to N₂.

On the other hand, carbon dioxide isotherm presents a promising adsorption capacity at 1 bar, highlighting the potential of this novel material in gas separation processes. The slightly shorter CO₂ kinetic diameter enable its diffusion along the framework, reaching a competitive adsorption capacity of 88 mL CO₂ per gram of sample, and with characteristic surface area values corresponding to 431 m² g⁻¹ (BET surface area) and 446 m² g⁻¹ (Langmuir surface area).

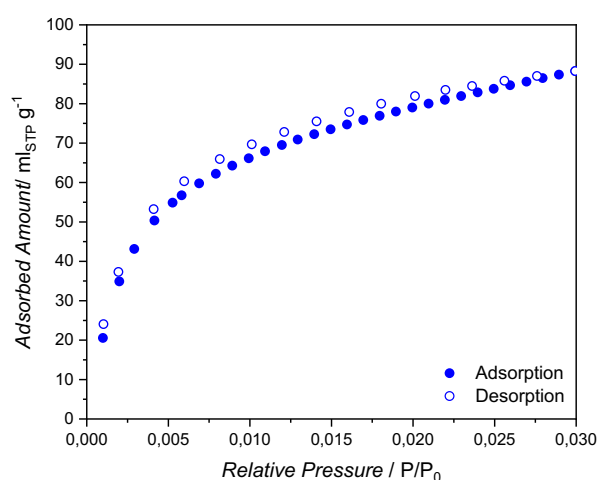


Figure S10. Single gas adsorption/desorption CO₂ isotherm on compound **1**, at 273 K (solid symbols for adsorption and open ones for desorption).

High-pressure gravimetric adsorption isotherms of CO₂, CH₄ and N₂ were measured at different temperatures, ranging from 283 to 318 K, in an IGA-100 gas sorption analyser (from Hiden Isochema) using approximately 50 mg of sample. Before each adsorption experiment, the sample was outgassed at 393 K under vacuum (10⁻⁵ Pa) for two hours. Equilibrium conditions corresponded to 600 s interval, and 0.001 mg min⁻¹ tolerance.

Kinetics study (Figure S8) on CO₂ high-pressure adsorption isotherms, reveals the impact of temperature in the behaviour of the gas-framework interaction. At low temperature (283-298 K) adsorption exhibits a steeper slope at the beginning of the profile (low pressure region), promoting an agile adsorption at low CO₂ concentrations.

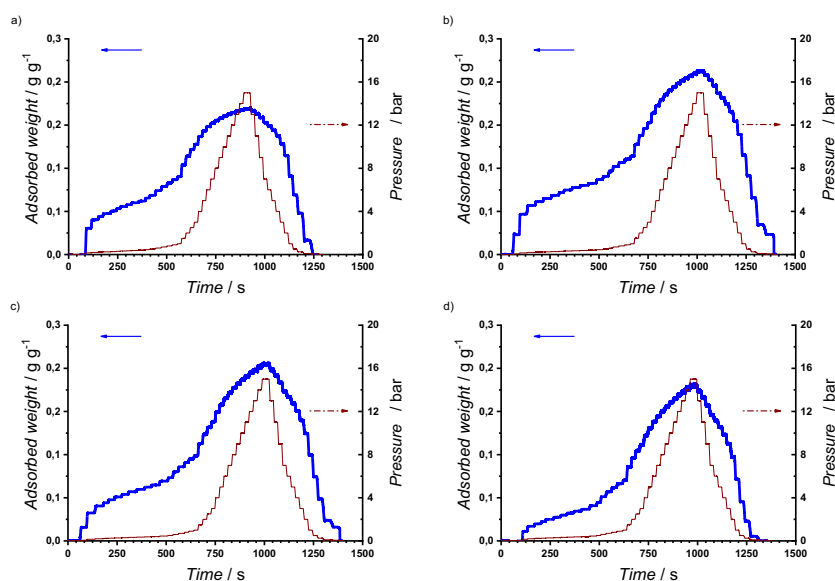


Figure S11. Isothermal kinetic study for CO₂ adsorption (pressure vs. time) in compound **1**, at 15 bar, at different temperatures: (a) 283 K, (b) 298 K, (c) 308 K, and (d) 318 K. Equilibrium conditions set to 600 s interval, with a tolerance of 0.001 mg min⁻¹.

For high-pressure CO₂ isotherms, virial equations were applied for fitting experimental data points, with a fourth-grade polynomial. In addition, heat of adsorption was calculated according to the Clausius-Clapeyron equation, through the data extracted from the experimental isotherms at different temperatures (Figure S12).

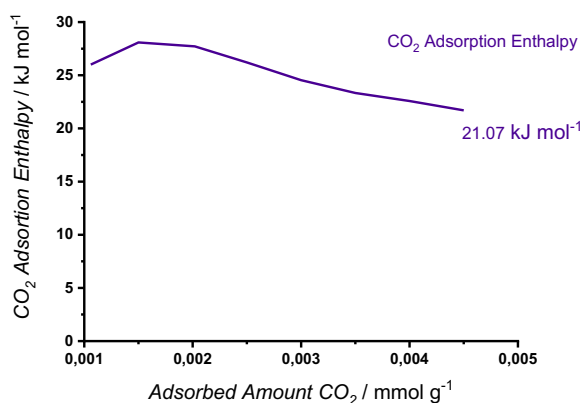


Figure S12. Isothermic heat of adsorption of CO₂ on compound **1**, according to the Clausius-Clapeyron equation.

b. Dynamic Adsorptive Separation Measurements

ABR (HIDEN Isochema), which stands for Automated Breakthrough Analyser, and corresponds to a setup based on a packed adsorption column, was used to study the

adsorption dynamics of pure gases and, especially, mixtures. Pressure, temperature and inlet composition are controlled, and the outlet composition is analysed, by an integrated mass spectrometer (HPR-20 QIC). The fixed-bed column was filled with 286 mg of compound **1**. Before each measurement, the sample was regenerated at atmospheric temperature and pressure, in 40 mL min⁻¹ Ar flow for 20 minutes. Operation conditions ranged 283-323 K, at 1 bar. The inlet mixture was set to a 15 mL min⁻¹ flow of a dilution of carbon dioxide in N₂ or CH₄ (5%, 20%, 50%). Time zero was set with the first detection of helium, which was used as a trace (an extra 1 mL min⁻¹ of He in the total feed flow of 16 mL min⁻¹). The expected roll-up phenomenon is observed in N₂, CH₄ and He profiles, as a double consequence of their increased MS signal intensity during CO₂ adsorption, and the actual carbon dioxide breaking effect.

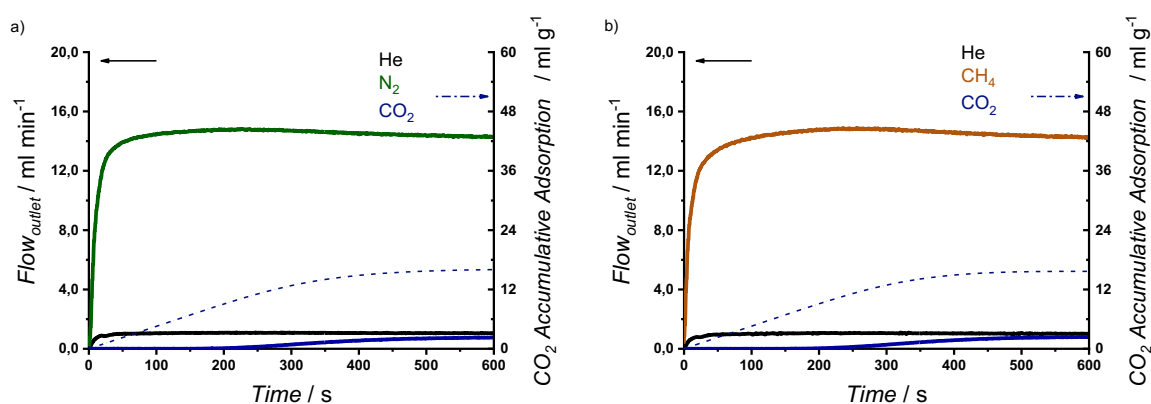


Figure S13. Breakthrough exit flowrates (solid line, left axis) and CO₂ accumulative adsorption (dash-dot line, right axis) vs. time at 283 K and 1 bar, on compound **1**. Inlet composition corresponds to a 5 % dilution of CO₂: (a) in nitrogen, and (b) in methane. Time zero is set with the first detection of helium (tracer).

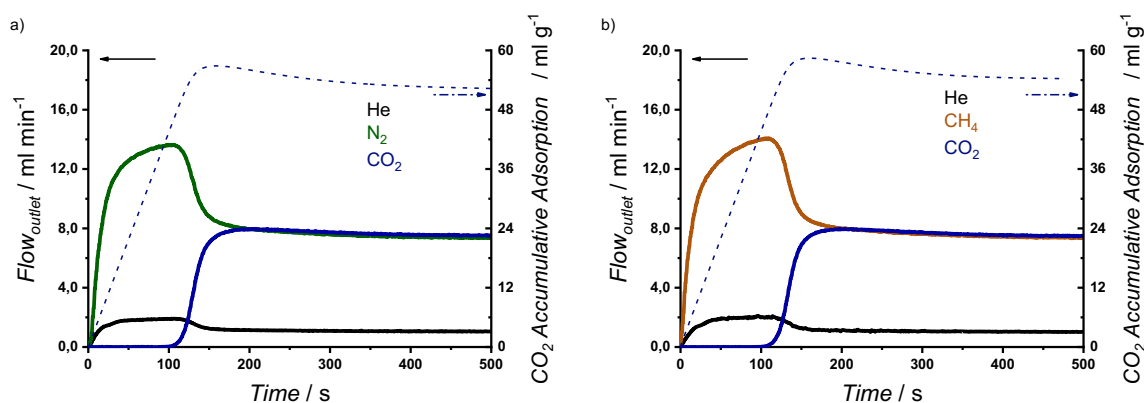


Figure S14. Breakthrough exit flowrates (solid line, left axis) and CO₂ accumulative adsorption (dash-dot line, right axis) vs. time at 283 K and 1 bar, on compound **1**. Inlet composition corresponds to a 50 % dilution of CO₂: (a) in nitrogen, and (b) in methane. Time zero is set with the first detection of helium (tracer).

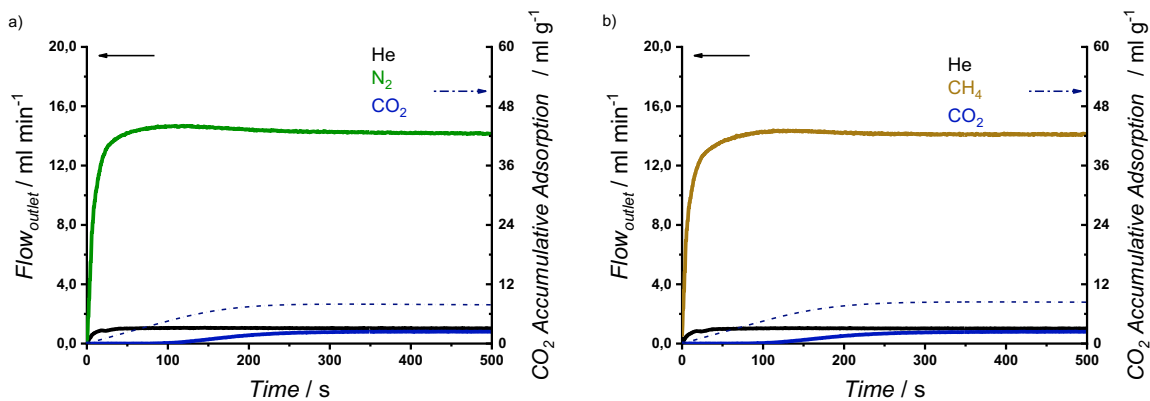


Figure S15. Breakthrough exit flowrates (solid line, left axis) and CO₂ accumulative adsorption (dash-dot line, right axis) vs. time at 298 K and 1 bar, on compound **1**. Inlet composition corresponds to a 5 % dilution of CO₂: (a) in nitrogen, and (b) in methane. Time zero is set with the first detection of helium (tracer).

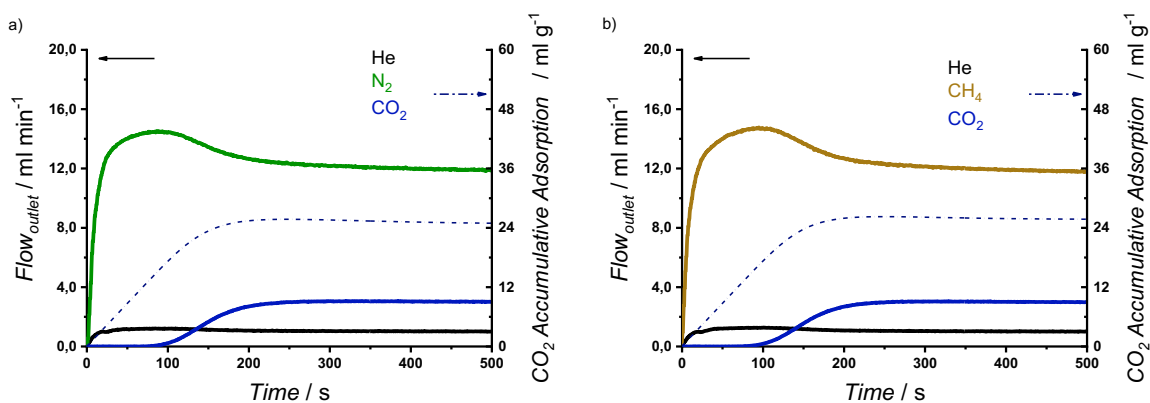


Figure S16. Breakthrough exit flowrates (solid line, left axis) and CO₂ accumulative adsorption (dash-dot line, right axis) vs. time at 298 K and 1 bar, on compound **1**. Inlet composition corresponds to a 20 % dilution of CO₂: (a) in nitrogen, and (b) in methane. Time zero is set with the first detection of helium (tracer).

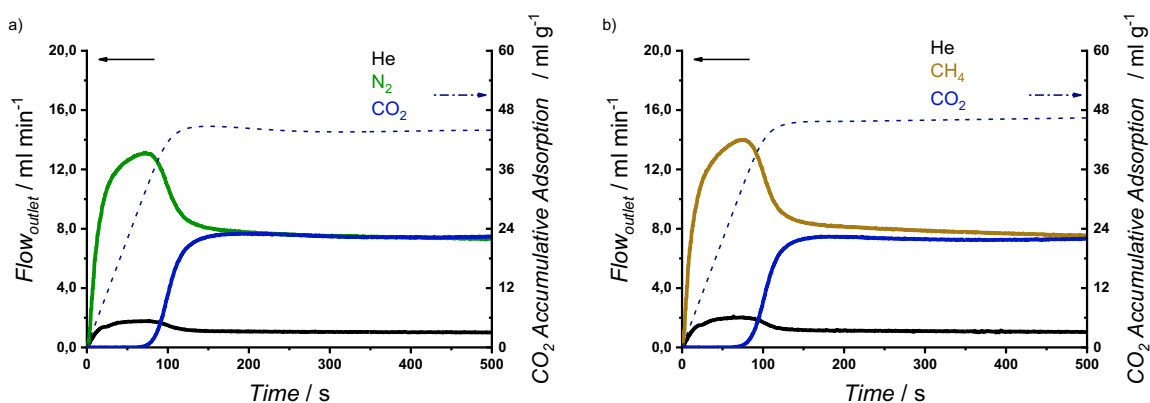


Figure S17. Breakthrough exit flowrates (solid line, left axis) and CO₂ accumulative adsorption (dash-dot line, right axis) vs. time at 298 K and 1 bar, on compound **1**. Inlet composition corresponds to a 50 % dilution of CO₂: (a) in nitrogen, and (b) in methane. Time zero is set with the first detection of helium (tracer).

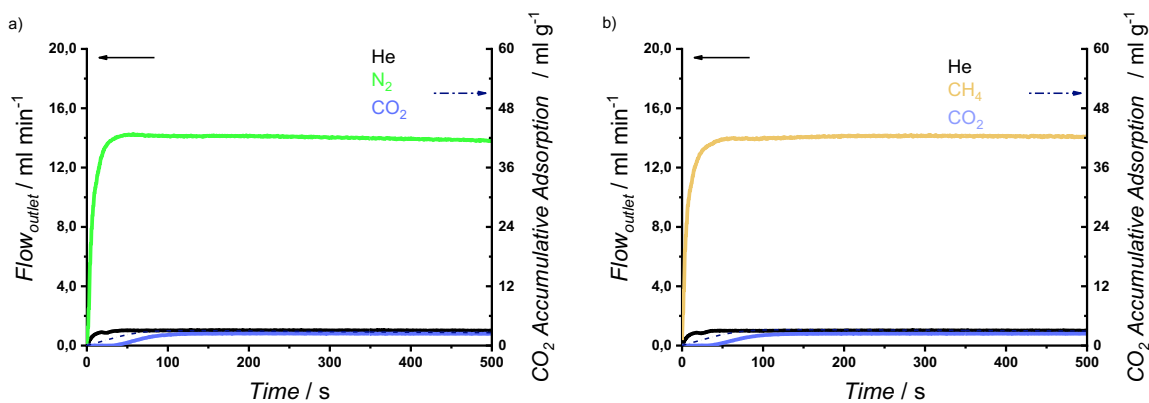


Figure S18. Breakthrough exit flowrates (solid line, left axis) and CO₂ accumulative adsorption (dash-dot line, right axis) vs. time at 323 K and 1 bar, on compound **1**. Inlet composition corresponds to a 5 % dilution of CO₂: (a) in nitrogen, and (b) in methane. Time zero is set with the first detection of helium (tracer).

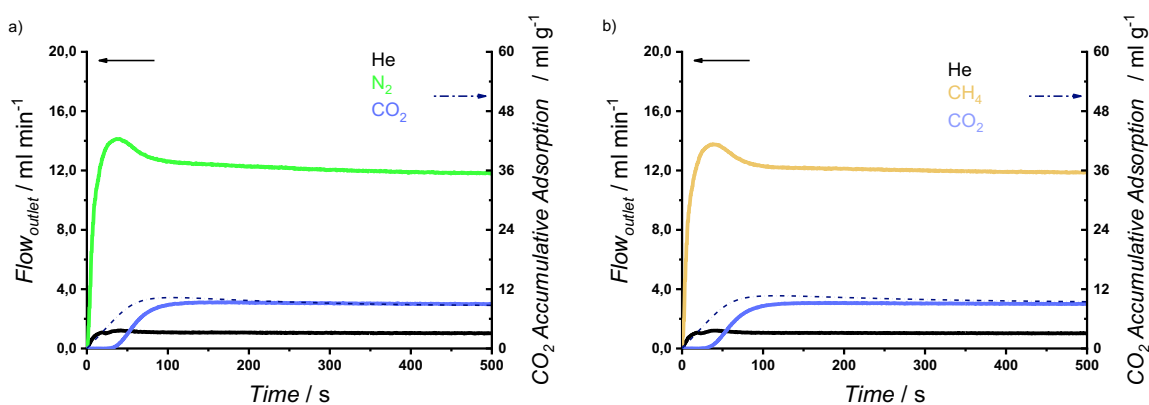


Figure S19. Breakthrough exit flowrates (solid line, left axis) and CO₂ accumulative adsorption (dash-dot line, right axis) vs. time at 323 K and 1 bar, on compound **1**. Inlet composition corresponds to a 20 % dilution of CO₂: (a) in nitrogen, and (b) in methane. Time zero is set with the first detection of helium (tracer).

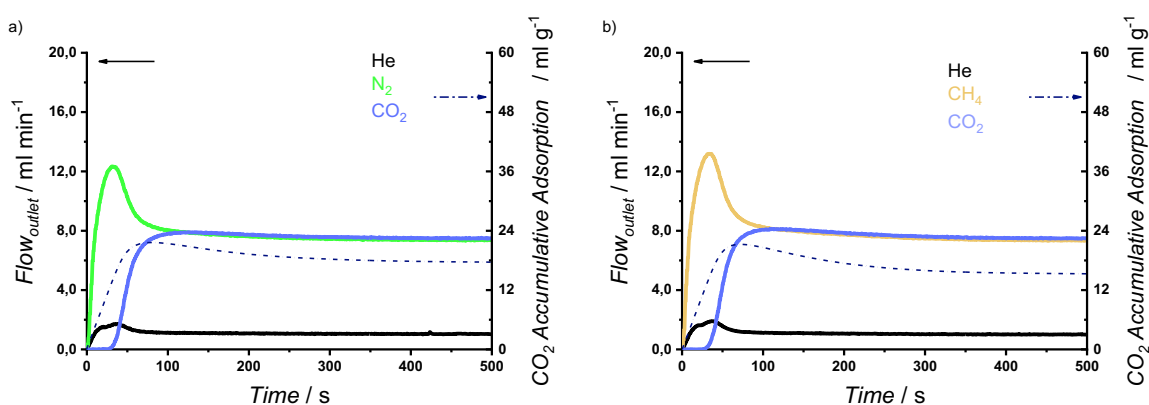


Figure S20. Breakthrough exit flowrates (solid line, left axis) and CO₂ accumulative adsorption (dash-dot line, right axis) vs. time at 323 K and 1 bar, on compound **1**. Inlet composition corresponds to a 50 % dilution of CO₂: (a) in nitrogen, and (b) in methane. Time zero is set with the first detection of helium (tracer).

It is known and accepted, that dynamic adsorption is always lower than under equilibrium (static) conditions. Table S3 displays the comparison of the experimental adsorption capacities from

isotherms (static conditions) and breakthrough measurements (dynamic conditions). In correlation with the exposed above about CO₂ adsorption kinetics, capacity values are closer at low temperature, where adsorption is promoted at low concentrations, and semi-equilibrium conditions are achieved in a short period of time.

Table S3. Comparison between static single gas adsorption capacities (extracted from equilibrium isotherms) and dynamic experimental adsorption capacities (determined from breakthrough measurements for CO₂: N₂ mixtures) for CO₂ on compound **1**, at different pressure (0.05 bar - 0.5 bar) and temperature (283 K – 318 K).

| Exp. conditions | CO ₂ adsorbed <i>static</i> (mL g ⁻¹) | CO ₂ adsorbed <i>dynamic</i> (mL g ⁻¹) | Comparison ratio % (-) |
|---------------------------------|--|---|------------------------------|
| 283 K; 0.05 bar CO ₂ | 23.9 | 16.1 | 68 % |
| 283 K; 0.2 bar CO ₂ | 52.1 | 39.9 | 77 % |
| 283 K; 0.5 bar CO ₂ | 68.4 | 52.2 | 76 % |
| 298 K; 0.05 bar CO ₂ | 12.3 | 8.0 | 65 % |
| 298 K; 0.2 bar CO ₂ | 34.8 | 25.7 | 74 % |
| 298 K; 0.5 bar CO ₂ | 55.3 | 43.9 | 79 % |
| 323 K; 0.05 bar CO ₂ | 5.9* | 3.0 | 51 % |
| 323 K; 0.2 bar CO ₂ | 17.3* | 8.7 | 50 % |
| 323 K; 0.5 bar CO ₂ | 34.4* | 17.5 | 51 % |

(* Isotherms performed at 318 K)

Regeneration of compound **1** was successfully achieved at mild conditions. **Figure S21** exhibits the PXRD patterns before and after adsorption measurements, validating the stability of the material. As every ABR experiment was performed twice, Figures S20-S21 display breakthrough profiles for the two replicas for one the set conditions (for CO₂:N₂ and CO₂:CH₄ mixtures, respectively); and Tables S4-S5 collect all the experimental data (adsorption amounts and selectivities) for each condition set, comparing the original result with its replica.

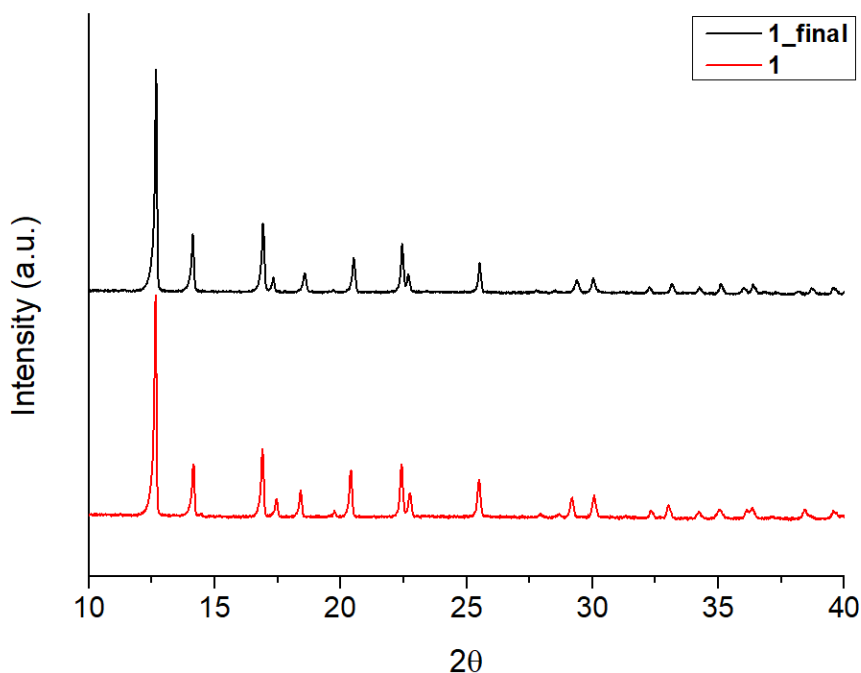


Figure S21. PXRD patterns of compound **1** before adsorption measurements (red) and compound **1** after completing adsorption study (black), in the range 10-40°.

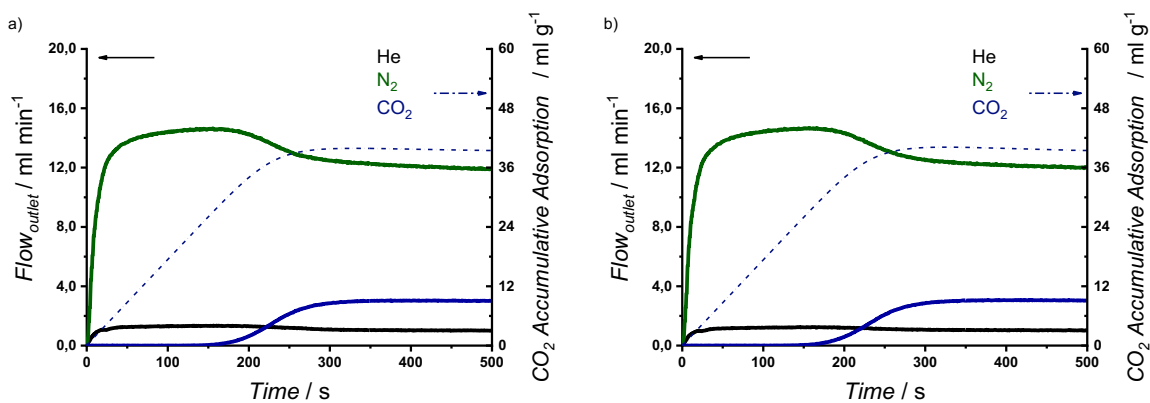


Figure S22. Breakthrough exit flowrates (solid line, left axis) and CO₂ accumulative adsorption (dash-dot line, right axis) vs. time at 283 K and 1 bar, on compound **1**. Inlet composition corresponds to a 20 % dilution of CO₂ in nitrogen: (a) original, and (b) replica. Time zero is set with the first detection of helium (tracer).

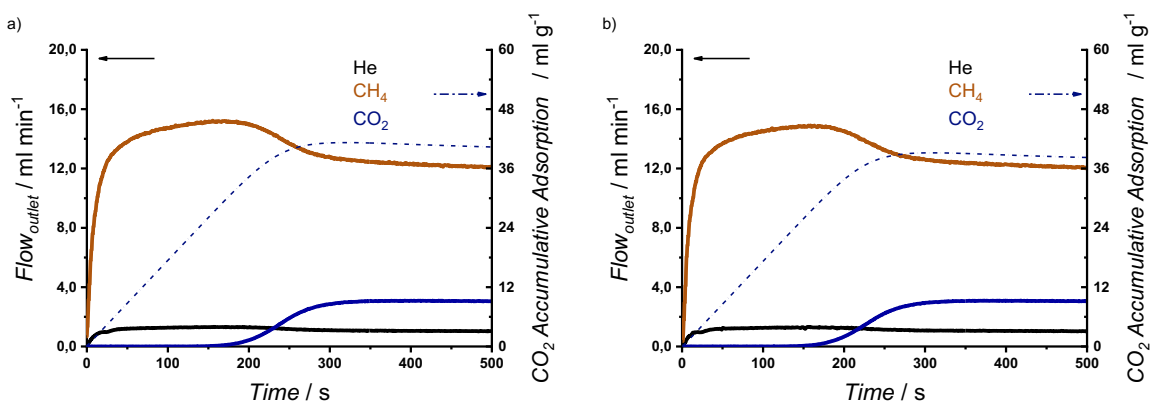


Figure S23. Breakthrough exit flowrates (solid line, left axis) and CO₂ accumulative adsorption (dash-dot line, right axis) vs. time at 283 K and 1 bar, on compound **1**. Inlet composition corresponds to a 20 % dilution of CO₂ in methane: (a) original, and (b) replica. Time zero is set with the first detection of helium (tracer).

Table S4. Experimental selectivities (α) for compound **1**, calculated from the integration of the respective breakthrough curves in CO₂:N₂ adsorptive separation. (original and replica measurements).

| Exp. conditions | CO ₂ adsorbed (mL g ⁻¹) | N ₂ adsorbed (mL g ⁻¹) | Selectivity (α) |
|----------------------------|---|--|--------------------------|
| 283 K; 5% CO ₂ | 16.1 | 0.0 | >1000 |
| 283 K; 5% CO ₂ | 15.1 | 0.0 | >1000 |
| 283 K; 20% CO ₂ | 39.9 | 0.0 | >1000 |
| 283 K; 20% CO ₂ | 40.1 | 0.0 | >1000 |
| 283 K; 50% CO ₂ | 52.2 | 0.0 | >1000 |
| 283 K; 50% CO ₂ | 54.6 | 0.0 | >1000 |
| 298 K; 5% CO ₂ | 8.0 | 0.2* | >500 |
| 298 K; 5% CO ₂ | 8.0 | 0.9* | 159 |
| 298 K; 20% CO ₂ | 25.7 | 0.0 | >1000 |

| | | | |
|----------------------------|------|-----|-------|
| 298 K; 20% CO ₂ | 26.0 | 0.0 | >1000 |
| 298 K; 50% CO ₂ | 43.9 | 0.0 | >1000 |
| 298 K; 50% CO ₂ | 39.8 | 0.0 | >1000 |
| 323 K; 5% CO ₂ | 3.0 | 5.3 | 10 |
| 323 K; 5% CO ₂ | 3.0 | 6.3 | 8 |
| 323 K; 20% CO ₂ | 8.7 | 0.0 | >1000 |
| 323 K; 20% CO ₂ | 9.4 | 0.0 | >1000 |
| 323 K; 50% CO ₂ | 17.5 | 0.0 | >1000 |
| 323 K; 50% CO ₂ | 17.3 | 0.0 | >1000 |

(*) negligible values

Table S5. Experimental selectivities (α) for compound **1**, calculated from the integration of the respective breakthrough curves in CO₂:CH₄ adsorptive separation. (original and replica measurements).

| Exp. conditions | CO ₂ adsorbed (mL g ⁻¹) | CH ₄ adsorbed (mL g ⁻¹) | Selectivity (α) |
|----------------------------|---|---|--------------------------|
| 283 K; 5% CO ₂ | 15.6 | 0.0 | >1000 |
| 283 K; 5% CO ₂ | 15.8 | 0.0 | >1000 |
| 283 K; 20% CO ₂ | 41.1 | 0.0 | >1000 |
| 283 K; 20% CO ₂ | 38.8 | 0.0 | >1000 |
| 283 K; 50% CO ₂ | 54.3 | 0.0 | >1000 |
| 283 K; 50% CO ₂ | 56.4 | 0.0 | >1000 |
| 298 K; 5% CO ₂ | 8.4 | 5.8 | 26 |
| 298 K; 5% CO ₂ | 8.2 | 4.8 | 30 |
| 298 K; 20% CO ₂ | 26.1 | 0.0 | >1000 |
| 298 K; 20% CO ₂ | 23.9 | 0.0 | >1000 |
| 298 K; 50% CO ₂ | 38.4 | 0.0 | >1000 |
| 298 K; 50% CO ₂ | 45.7 | 0.0 | >1000 |
| 323 K; 5% CO ₂ | 3.1 | 6.8 | 8 |
| 323 K; 5% CO ₂ | 3.2 | 9.6 | 6 |
| 323 K; 20% CO ₂ | 10.5 | 0.0 | >1000 |
| 323 K; 20% CO ₂ | 12.5 | 0.0 | >1000 |
| 323 K; 50% CO ₂ | 18.7 | 0.0 | >1000 |
| 323 K; 50% CO ₂ | 20.2 | 0.0 | >1000 |

7. Stability studies

The robustness of the material was also evaluated by performing gravimetric measurements of the CO₂ adsorption, measuring the sample after all the gas separation studies were performed (40 different breakthrough separation studies with regeneration) and the sample was stored in a closed vial under air atmosphere at room temperature for 3 months. The sorption capacity of the material is mostly retained (see **Table S6** and **Figure S24**).

Table S6. CO₂ sorption capacity at 6 bar and 283 K of the original sample before and after gas separation studies, with 3 months of storage between the measurements.

| Sample | CO ₂ Sorption Capacity / mmol·g ⁻¹ |
|-----------------|--|
| Original Sample | 5.4 |
| After 3 Months | 4.9 |

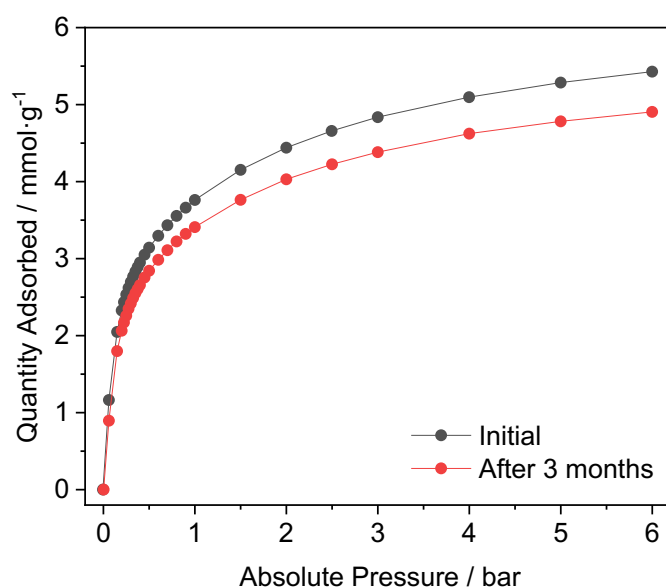


Figure S24. CO₂ adsorption isotherms at 283 K of the initial material and the sample after performing all the separation studies (40 different breakthrough separation studies with regeneration). Before CO₂ adsorption isotherm, samples were activated at 150 °C for 2 hours.

To evaluate the chemical stability of the material, the product was divided in three aliquots (50 mg each) and soaked in different solutions (10 mL) with pH values adjusted at pH = 1, 7 and 12 for 3 hours. The materials were then washed three times with MeOH and collected by centrifugation (8000 rpm, 10 min at RT) and left to dry in air overnight.

The porosity of the samples was evaluated by CO₂ sorption measurements after activation at 150 °C for 2h. The CO₂ sorption capacity of the material (**Figure S25**) is not affected after this study, as the material retains the same amount of CO₂ with minor differences in the CO₂ sorption isotherms

attributed to performing different experiments. The sorption capacity for each sample is resumed in **table S7**.

The robustness and of the framework was assessed after the solvent treatment and gas sorption measurements, by performing PXRD measurements of the treated materials (**Figure S25**). The crystalline structure of the samples after the solvent treatment is retained in all the cases.

Table S7. CO₂ sorption capacity at 1 bar and 273 K of the pristine material and treated samples.

| Sample | CO ₂ Sorption Capacity / mmol·g ⁻¹ |
|-------------------|--|
| Pristine Material | 3.8 |
| pH = 1 | 3.7 |
| pH = 7 | 3.9 |
| pH = 12 | 3.8 |

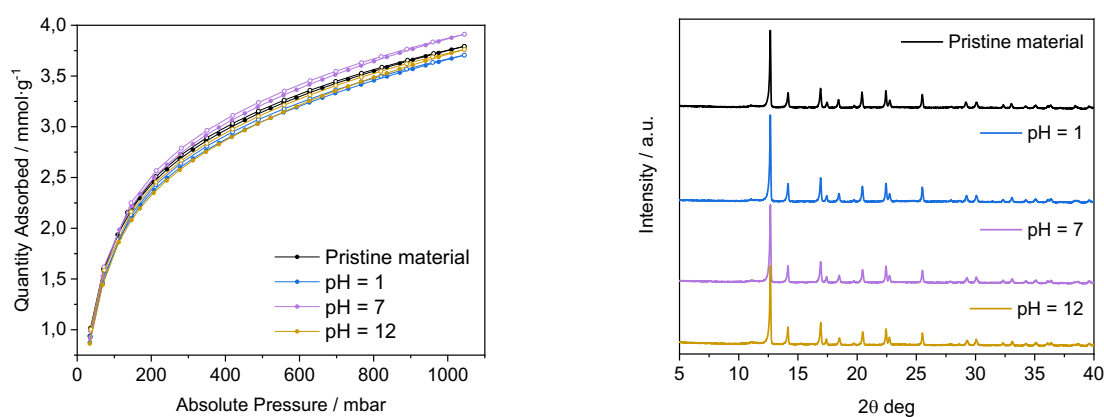


Figure S25. CO₂ sorption isotherms at 273 K of the pristine and treated materials activated at 150 °C for 2 hours (solid symbols for adsorption and open ones for desorption) (left) and PXRD patterns of the pristine material and the treated samples after CO₂ sorption measurements (right).

8. References

- 1 W. Gauß, H. Heitzer and S. Petersen, *Justus Liebigs Ann. Chem.*, 1973, **764**, 131–144.
- 2 F. M. A. Kerim, H. F. Aly and A. El-Agramy, *Proc. Indian Acad. Sci. - Sect. A*, 1977, **85**, 559–566.

- 3 M. K. Trivedi, R. M. Tallapragada, A. Branton, D. Trivedi, G. Nayak, R. K. Mishra and S. Jana, *J. Mol. Pharm. Org. Process Res.*, 2015, **03**, 1–6.
- 4 O. Roubeau, B. Agricole, R. Cle and S. Ravaine, *J. Phys. Chem. B*, 2004, **108**, 15110–15116.
- 5 Q. Deng, C. Tian, Z. Luo, Y. Zhou, B. Gou, H. Liu, Y. Ding and R. Yang, *Chem. Commun.*, 2020, **56**, 12234–12237.
- 6 G. M. Sheldrick, *Acta Crystallogr. Sect. A Found. Crystallogr.*, 2015, **71**, 3–8.
- 7 G. M. Sheldrick, *Acta Crystallogr. Sect. C Struct. Chem.*, 2015, **71**, 3–8.
- 8 O. V. Dolomanov, L. J. Bourhis, R. J. Gildea, J. A. K. Howard and H. Puschmann, *J. Appl. Crystallogr.*, 2009, **42**, 339–341.
- 9 S. Kawata, S. Kitagawa, H. Kumagai, T. Ishiyama, K. Honda, H. Tobita, I. Keiichi Adachi and M. Katada, *Chem. Mater.*, 1998, **10**, 3902–3912.
- 10 L. Liu, J. A. Degayner, L. Sun, D. Z. Zee and T. D. Harris, *Chem. Sci.*, 2019, **10**, 4652–4661.
- 11 M.E. Fisher, *J. Math. Phys.*, 1963, **4**, 124-135.